PROCEEDINGS OF THE INTERNATIONAL CONFERENCE ON NEWVIEWS IN ENGINEERING AND TECHNOLOGY (ICNET) MAIDEN EDITION, FACULTY OF ENGINEERING, RIVERS STATE UNIVERSITY, PORT HARCOURT, NIGERIA.
27th October 2021
Available online at https://conference.rsujnet.org/

Paper number: ICNET2021-022

Recovery of Lead (II) Ion from Industrial Wastewater using Activated Periwinkle Char in Fixed Bed Adsorption Process

Babalola R.[1] and Aniediong U.[2]
[1,2]Department of Chemical/Petrochemical engineering, Faculty of Engineering, Akwaibom state university, Akwalbom State, Nigeria.
rasheedbabalola@aksu.edu.ng, +234 803 159 2001.

ABSTRACT
The discharge of untreated industrial wastewater containing lead and the indiscriminate disposal of periwinkle shell causes lead poisoning and blockage of drainage. The cost of industrial wastewater treatment is demanding; thus the research is focused on creating wealth from waste periwinkle shell as a cheap adsorbent material to reduce the cost of lead removal from industrial wastewater. Therefore, activated periwinkle shell char (APSC) in removal of lead Pb (II) ion from industry wastewater was investigated using fixed-bed adsorption column. APSC was prepared by treating the periwinkle Char with 1M H_2SO_4 solution. Characterization of the adsorbent before and after continuous adsorption was performed using Fourier transform infrared spectroscopy (FTIR) and Scanning electron microscopy (SEM) to show modifications in the surface and chemical structure of APSC after adsorption process. The effect of design variables such as bed height, Influent concentration and withdrawal flowrate were studied. The breakthrough profiles were obtained by an analysis of the column experimental data and the relationship between operating parameters using the Thomas, Clark, Yoon-Nelson and Adams-Bohart models. The equilibrium data was best represented by the Yoon and Nelson model having the highest correlation coefficient (R^2) of 0.9751. This suggest that Activated periwinkle shell char is a potential adsorbent for heavy metals removal from industrial wastewater.

KEYWORDS: activated, adsorption, char, periwinkle**.**

Cite This Paper: Babalola R. & Aniediong U. (2021). Recovery of Lead (II) Ion from Industrial Wastewater using Activated Periwinkle Char in Fixed Bed Adsorption Process. *Proceedings of the International Conference on Newviews in Engineering and Technology Maiden Edition*, Faculty of Engineering, Rivers State University, Port Harcourt. Nigeria, 27th October 2021, ICNET2021-022, 217 – 227.

1. INTRODUCTION

Communities in industrial areas are facing the challenge of save and healthy drinking water due to the discharge of untreated industrial wastewater into the environment. To contend with these challenges, regulatory bodies have come up with standard for treatment of industrial wastewater and stiff punishment for violators because of the adverse effect of these pollutants, evidence are established in the National Environmental Regulations (National Environmental Standard and Regulations Enforcement Agency, 2009; Ministry of Environment , 1999). Lead is a priority pollutant; it finds its way into the receiving water body majorly through industrial wastewater, they bio-accumulate in the tissues of the marine lives and translocate to humans through food chains. Consequently, Lead poisoning occur leading to mental retardations, kidney malfunctioning and anaemia (Mohsen *et al.*, 2015; Uzoije & Uche, 2016).

Aimikhe and Lekia (2021) related that in coastal communities' periwinkle is a major source of proteins in most delicacies. It shells contribute to environmental degradation because of the indiscriminate disposal blocking drainages. They reviewed the various way by which periwinkle shell can be processed and utilized, including its use as an

Copyright © 2019 – 2021 JNET-RSU, All right reserved

adsorbent material. The studies of Fe^{3+} ion removal from aqueous solutions using periwinkle shell activated carbon was investigated by Akpa and Ndukam (2018). The thermodynamic parameters results showed that adsorption process was endothermic with Enthalpy change (ΔH˚): 222.91 kJ/mol; a positive Entropy change (ΔS˚) of 19.19 kJ/mol, indicating an increase in the degree of freedom (or disorder) of the adsorbed species and a negative Gibb's free energy (ΔG˚) at all temperature indicating that the adsorption process was spontaneous and favorable at high temperature.

Mohsen *et al.* (2015) reviewed various methods for lead removal from industrial wastewater including chemical precipitation, electrochemical reduction, ion exchange, reverse osmosis, membrane separation, and adsorption. Based on technical applicability, plant simplicity and cost-effectiveness, they concluded that adsorption is the most effective method. Uzoije and Uche (2016) investigated the dynamic adsorption process of Pb (II) iononto fixed-beds plantain peel activated carbon (PPAC) and bamboo activated carbon (BAC) materials to treat vegetable oil polluted wastewater. The capacity of these materials to adsorb Pb (II) ion increased with increase in initial concentration and bed height but decreased as inflow rate increase, decrease in initial concentration and bed height. Their data were fitted into Thomas, Adams Bohart, Yoons and Nelson dynamic adsorption models to determine the extent of compatibility. Thomas model was most complied followed by Yoon-Nelson model whereas the least complied model was Adams-Bohart.

This research is focused on creating wealth from waste periwinkle shell as a cheap adsorbent material to reduce the cost of lead removal from industrial wastewater. Therefore, the objective of the paper is to characterize APSC adsorbent before and after the adsorption of lead, to investigate the effect of design variables such as bed height, influent concentration and withdrawal flowrate by analysis of the column experimental data and the relationship between operating parameters using the Thomas, Clark, Yoon-Nelson and Adams-Bohart models.

2. MATERIALS AND METHODS

2.1. Materials.

Periwinkle shells were obtained from Ukam market. The chemicals used in the experiment were of analytical reagent grade. Sulphuric acid (98%, Aldrich), Lead nitrate (99%, Aldrich), Hydrochloric acid (99.5%, Lab Tech Chemicals) and sodium hydroxide (99.5%, Phillip Harris). A stock solution of 1000 mg/l was prepared through dissolution of appropriate amount of $Pb(NO_3)_2$ salt in deionized water. The stock solution was diluted to obtain the required concentrations used in the experiment.

2.2. Preparation of Adsorbent.

The adsorbent was prepared by first washing the periwinkle shells with distilled water to remove dirt and soil debris. The clean shells were sun-dried for 2 days and oven dried for 3 hours. It was carbonized in a tubular muffle furnace for 1 hr 30 min at 800 °C. Then, the materials were crushed into smaller particle sizes with the aid of a mortar and a pestle. Next, the material was chemically impregnated with aratio of 2:1 using a 1M solution of sulphuric acid. It was allowed to stay for 48 h and was further heated in furnace at 900°C for 1 hr 30 min using the muffle furnace. 0.1M sodium hydroxide (NaOH) and 0.1M Hydrochloric acid (HCl) were used to stabilize the pH. The prepared adsorbent is presented in Figure 1.

Copyright © 2019 – 2021 JNET-RSU, All right reserved

Figure 1. Activated Periwinkle Shell Char

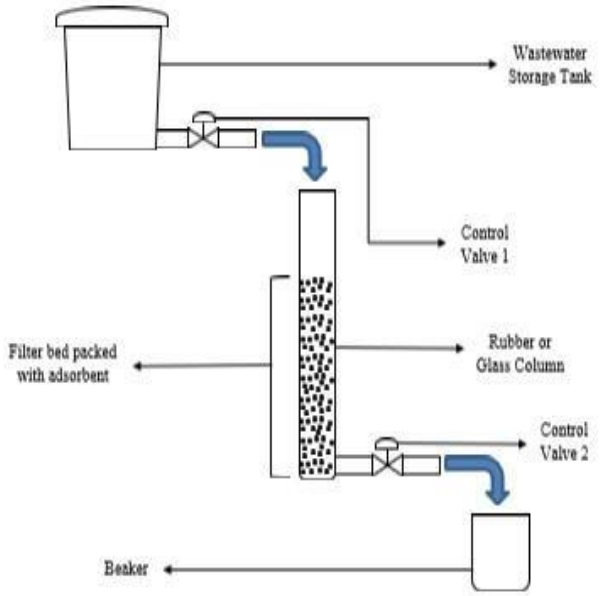

Figure 2: Basic design of column adsorption

2.3 Analysis and Characterization.

The granulometric curve of the APSC and the simple percentages (%) of each granular fraction were established using a vibrating sieve shaker (RETSCH AS 200). The concentrations of the lead ion in the solutions were determined by using atomic absorption spectrophotometer (Perkin Elmer Model AAS 700). The pH meter (Hach) was used to determine the pH of the sample, while Functional groups of the adsorbent were identified by the Fourier transform infrared spectroscopy (FTIR) (Bruker 3000 Hyperion, Germany). Morphological analysis of the adsorbent was done by using the scanning electron microscope (SEM) (JELO JSM7600F), (Oxford Aztec energy system).

*2.4.*Process Description.

Dynamic column studies were carried out in a rubber column of 6.80 cm internal diameter and 35 cm height. The adsorbent bed were packed into the column and wetted with distilled water to release the trapped air between the particles. Industrial wastewater was continuously supplied through the column using the influence of gravity; installed valves were used to maintain the desired influent and effluent flow rate. Experiments were carried out at room temperature 28 ± 1 °C. Effects of process parameter like withdrawal flowrates (5, 7, and 10 mL/min), bed depth (3, 5, and 7 cm) and concentration (10, 50, and 100 mg/L) were investigated. Samples were collected at predefined time intervals from the bottom of the column and were tested to know the lead concentration. Figure 2represents a basic design of adsorption column.

3. RESULTS AND DISCUSSION

3.1 Adsorbent Granulometry Result.

The descriptive percentages of the granulometric analysis are illustrated in Figure 3. The graph shows the allocation of 6 fractions for the granulometric distribution of APSC, and the preponderant size which predominates is 1 mm with a percentage of 49.1%. This size is greater

Copyright © 2019 – 2021 JNET-RSU, All right reserved

than 0.5 mm but less than 2mm, which gives it a medium class.

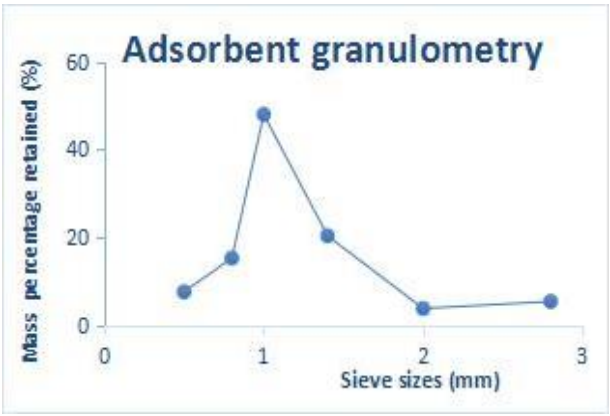

Figure 3: Granulometric curve of prepared Adsorbent

3.2. Fourier Transform Infrared Spectroscopy (FTIR) Result.

The spectra of the adsorbents were measured in the wave number range of 1000-3500 cm^{-1}as shown in Figure 4. The FTIR spectrum of APC implies the presence of predominant peaks at 3052.8 cm^{-1} (–OH and – NH stretching), 2516.0 cm^{-1} (–OH stretching), 2107.0 cm^{-1} (-C≡C- stretching), 1756.5 cm^{-1} (– C=O Stretching). Other notable peaks are summarized in Table 1.

It is visible from the Table 1 that all functional groups present are readily available for interaction with heavy metals. The observation proves that functional groups such as NH and OH are involved in binding heavy metal ions to APSC. After the adsorption process the shifting of the peaks was observed which further affirms that the adsorption process actual took place Figure 5. The major shifts in peaks found were from 3052.8 to 2508.5 cm-1(for –OH and –NH stretch), 2516.0 to 2105.9 cm-1 (for –OH stretch), 2107.0 to 1871.1 cm-1 (for $-C \equiv C-$), 1156.6 to 1095.8cm-1 (for C-H bend).

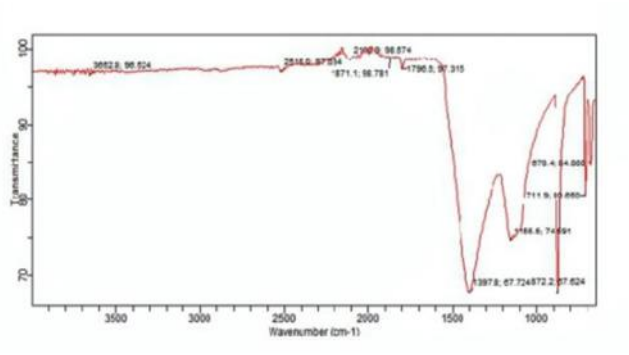

Figure 4: FTIR spectra of the adsorbent before adsorption experiment

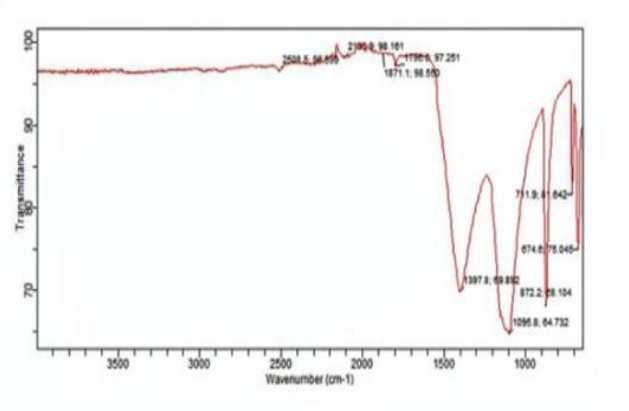

Figure 5: FTIR spectra of the adsorbent after adsorption experiment

3.3 Scanning Electron Microscopy (SEM) Result.

The internal microstructure of unused adsorbent shows a rough, irregular, and proportionally porous and cracked appearance with the presence of some luminous and relatively ordered fragments which allows the interchanges of substances with adjacent cells and thus makes the adsorption mechanism possible (Figure 6). Microstructural analysis reveals significant changes in the surface morphology of the adsorbent after the adsorption of lead. A dense and compact matrix with a decrease in the degree of porosity and luminosity was noticed, and this can be explained by the adsorption of the molecules contained in the treated

Copyright © 2019 – 2021 JNET-RSU, All right reserved

solute on the adsorbent cracks and pores (Figure7).

Table 1: Summary of FTIR spectra bond, frequencyand functional group

Frequency, cm^{-1}	Bond	Functional group
3052.8 (s, m)	O-H Stretch and N-H Stretch	Alcohol/Phenols, Amine/Amides
2516 (m)	O-H Stretch	Carboxylic acids
2107.0 (w)	- C ≡ C -	Alkynes
1756.5 (s)	- C = O Stretch	Carbonyls
1397.8 (w, m)	N-H bend	Amines
1156.6	C-H	Alkanes

m = medium, w = weak, s = strong

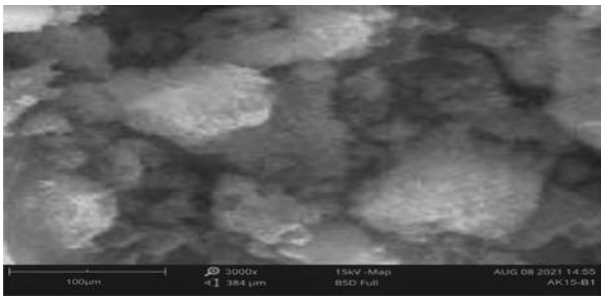

Figure 6: SEM photograph of prepared adsorbent at 3000x

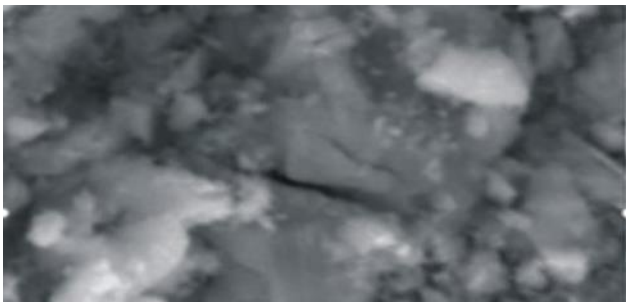

Figure 7: SEM photograph of the adsorbent after adsorption at 3000x

3.4. Absorption Spectroscopy (Lead Analysis) Result

From the results of the elemental analysis of the treated wastewater samples, the Table2 was created

3.4. Column Experiment Result

3.4.1 Effect of Bed Height on Lead Adsorption

Breakthrough curves obtained at different bed depth (3, 5, and 7 cm) with a constant influent concentration of 1.426 mg/L and withdrawal flow rate of 5 mL/min are shown in Figure 8. From the Figure 8, it is observed that time of breakthrough and time of exhaustion increases with increasing bed depth. At the lowest bed depth there is no sufficient time for lead ions to diffuse into the holes of APSC. A similar tendency is also reported in the work of Mondal Mondal (2009) who also attested to the fact that at smaller bed depths there is little interaction between the adsorbent and wastewater to be remedied.

Copyright © 2019 – 2021 JNET-RSU, All right reserved

Table2: Parameters in fixed bed column for lead adsorption by Activated periwinkle shell

Co (mg/l)	Qw (ml/min)	Z (cm)	MA (g)	C @5mins (mg/l)	C@30mins (mg/l)	C@60mins (mg/l)	C@180mins (mg/l)	C@300mins (mg/l)
10	5	5	168.5	2.085	2.934	3.371	4.868	6.248
50	5	5	167.9	14.947	18.684	25.590	31.769	39.613
100	5	5	168.2	46.891	59.747	71.392	80.671	95.955
1.426	5	5	169.0	0.384	0.414	0.498	0.572	0.775
1.426	7	5	168.4	0.423	0.456	0.523	0.727	0.895
1.426	10	5	168.0	0.492	0.536	0.632	0.802	1.007
1.426	5	3	101.8	0.517	0.545	0.692	0.937	1.122
1.426	5	5	168.6	0.405	0.433	0.509	0.688	0.915
1.426	5	7	227.2	0.373	0.395	0.452	0.521	0.704

3.4.2 Effect of Withdrawal Flowrate on Lead Adsorption

Breakthrough curves obtained at different withdrawal flowrate (5, 7, and 10ml/min) with a constant influent concentration of 1.426 mg/L and adsorbent bed height of 5cm are shown in Figure 9. From the plot it is observed that time of breakthrough and time of exhaustion increases with the decreasing withdrawal flowrate, which is expected since the increase in withdrawal flowrate causes a rapid saturation of the adsorption bed due to the increase in exchange speed

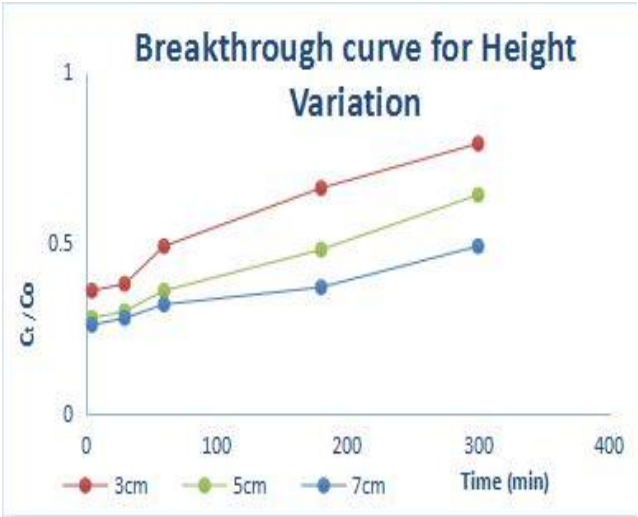

Figure 8: Breakthrough curve under varying bed heights

Copyright © 2019 – 2021 JNET-RSU, All right reserved

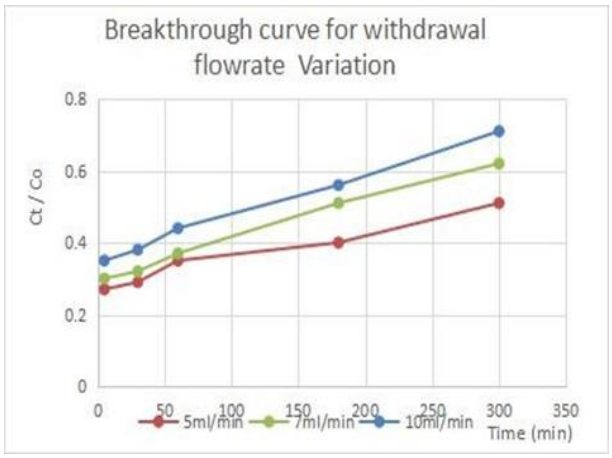

Figure 9: Breakthrough curve under varying withdrawal flowrates

3.5.3 Effect of Concentration dosage on lead adsorption on lead adsorption

Breakthrough curves obtained at different concentration dosages (10, 50, and 100mg/l) with a constant adsorbent bed height of 5cm and withdrawal flow rate of 5 mL/min are shown in Figure 10. From the plot it is observed that time of breakthrough and time of exhaustion increases with decreasing concentration dosages, and this makes sense since a higher concentration dosage would fill up the available active sites for adsorption faster. The findings of this study agree with the work of Cruz-Olivares, et al. (2013) who had a similar result in their work.

3.6 Continuous Adsorption Isotherm Modelling

The isotherm models used in correlating the equilibrium data obtained from this experiment includes the Thomas model, Bohart-Adams model, Yoon and Nelson model and the Clark model. After computing the values of the parameters for each model, the average R^2 value obtained from each of the models will be compared to determine the isotherm model that best fits this adsorption process.

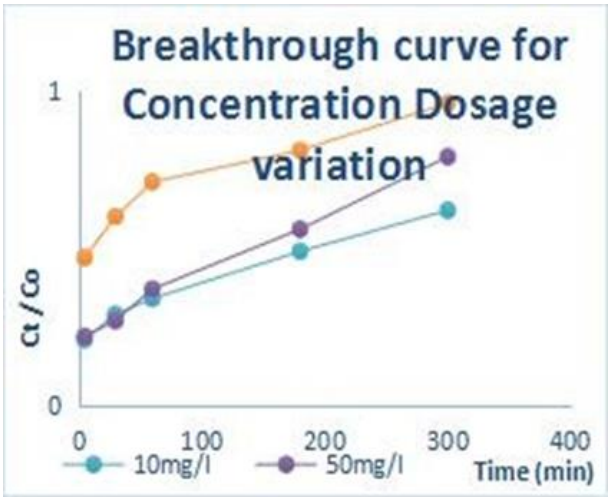

Figure 10: Breakthrough curve under varying Concentration dosages

3.6.1 Bohart-Adams Model

The experimental data Table 3 was fitted to Bohart-Adams model Eq. (1) to investigate its compliance with lead (II) ions adsorption process on Activated periwinkle shell char

$$ln\left[\frac{C_t}{C_0}\right] = K_{BA}C_0t - K_{BA}N_0\frac{Z}{Q} \qquad (1)$$

Were C_0 and C_t are the influent and effluent concentration, t is time, K_{BA} is the mass transfer coefficient, N_0 is the saturation concentration, Z is the bed height and Q is the influent flowrate. The constant in the model were estimated by plotting $ln\left[\frac{C_t}{C_0}\right]$ against t the mass transfer coefficient was obtained from the slope of the graph while the saturation concentration (N_0) was obtained from the intercept. It was observed from the result, Table 3 that the mass transfer coefficient increases with the increase in bed height and influent flowrate, while the saturation concentration increased as the influent concentration, flowrate and bed height increases.

This agrees with the experiment on the sorption of Mn(II) ions by using mangostanagarcinia peel-based granular-

Copyright © 2019 – 2021 JNET-RSU, All right reserved

activated carbon (Chowdhurt, et al., 2012) and the experiments on adsorption of Pb (II) ion using activated carbon of plantain peels and bamboo (Uzoije & Uche, 2016). Bohart-Adams has a lower correlation coefficient compared to other models and this agrees with the observation of previous research.

3.6.2 Yoon and Nelson Model

The experimental data Table 4 was fitted to Yoon and Nelson model Eq. (2) to investigate its compliance with lead (II) ions adsorption process on APSC.

$$ln\left[\frac{C_t}{C_0 - C_t}\right] = K_{YN}t - \tau K_{YN} \qquad (2)$$

Where K_{YN} is the rate constant and τ is the time required for 50% adsorbent break through. The constant in the model were estimated by plotting $ln\left[\frac{C_t}{C_0-C_t}\right]$ against *t*, $K_{YN}$was obtained from the slope of the graph while τ was obtained from the intercept. It was observed in Table 4 that with the increase in influent concentration and flowrate, theK_{YN} value increased while the value of τ decreased. This agrees with the results of the experiment carried out by Lopamudra et al.(2021). This is due to the fact that increase in influent concentration increases the competition between adsorbate molecules for the adsorption site resulting in increased uptake rate (Nwabanne, Okoye, & Lebele-Alawa, 2011). This model had the highest correlation coefficient compared to other models.

3.6.3 Thomas Model

The experimental data Table 5 was fitted to Thomas model Eq. (3) to investigate its compliance with lead (II) ions adsorption process on APSC.

$$ln\left[\frac{C_0}{C_t} - 1\right] = \frac{K_{th}q_{th}M}{Q} - K_{th}C_0t \qquad (3)$$

Where $K_{th}, q_{th}, MandQ$ represent Thomas adsorption constant, maximum adsorption capacity, and the influent flowrate respectively.

The $K_{th}\ and\ q_{th}$ were estimated from the slope and intercept of $ln\left[\frac{C_0}{C_t} - 1\right]$ against *t.*

it was observed from Table 5 that the increase in the packed bed height resulted in an increased in the maximum adsorption capacity of the system. Uzoije and Uche (2016) attributed this to broadening of mass transfer zone as a result of increasing the bed height.

3.6.4 Clark Model

The Thomas Clark model is expressed in Eq. (4)

$$ln\left[\left(\frac{C_0}{C_t}\right)^{n-1} - 1\right] = lnA - rt \qquad (4)$$

Where the values of A and r are obtained from the slope and intercept of $ln\left[\left(\frac{C_0}{C_t}\right)^{n-1} - 1\right]$ vs t. The experimental data was fitted to the Clark model, the results Table 6 indicated that an increase in the influent concentration increased the values of *A* and decreased the value of *r*. while influent flowrate has a reverse effect. The prediction of effluent concentration by the Clark model has a good correlation coefficient.

4.0 CONCLUSION

The study concluded that removal of lead ion in a fixed bed system using APSC is an effective and feasible method. The FTIR spectrum of APSC indicated the presence of predominant peaks and after the adsorption process the shifting of the peaks was observed which further affirms that the adsorption process actual took place. Additionally, the *SEM* microstructural analysis reveals significant

Copyright © 2019 – 2021 JNET-RSU, All right reserved

changes in the surface morphology of the adsorbent after the adsorption of lead

The behaviour of breakthrough curves and lead removal efficiency were strongly influenced by withdrawal flowrate, bed depth and influent concentration. The prediction of breakthrough curves was obtained by using Adams-Bohart, Thomas, Clark and Yoon-Nelson model. However, the entire breakthrough curve was best predicted by Yoon and Nelson model with an average R^2value of 0.9751.

REFERENCES

Aimikhe, V., & Lekia, G. (2021). An Overview of the Applications of Periwinkle (Tympanotonusfuscatus) Shells. *British Journal of Applied Science & Technology, 40*(18), 31-58.

Akpa, J. G., & Nduka, C. (2018). Kinetics, Equilibrium and Thermodynamics Studies of Fe3+ Ion Removal from Aqueous Solutions Using Periwinkle Shell Activated Carbon. *Advances in Chemical Engineering and Science, 8*, 49-66.

Chowdhurt, Z., Zain, S., Rashid, A., Rafique, R., & Khalid, K. (2012). Breakthrough Curve Analysis for Column Dynamics Sorption of Mn (II) Ions from Wastewater by Using Mangostanagarcinia Peel-Based Granular-Activated Carbon. *Journal of Chemistry*.

Cruz-Olivares, J., Perez-Alonso, C., Barrera-Diaz, C., i. Urena- Nunez, C., Chaparro-Mercado, C., & Bilyeu, B. (2013). Modeling of Lead (II) Biosorption by Residue of Allspice in a Fixed-bed Column. *Chemical Engineering Journa, 228*, 21-27.

Lopamudra, D., Saptarshi, S., Papita, D., Avijit, B., & Chiranjib, B. (2021). Experimental and Numerical modeling on dye adsorption using pyrolyzed mesoporous biochar in Batch and fixed-bed column reactor: Isotherm, Thermodynamics, Mass transfer, Kinetic analysis. *Surface and Interfaces, 23*.

Ministry of Environment. (1999). *National Environment (Standards for Discharge of Effluent.* Government of Ughanda.

Mohsen, A., Sara, H., & Masoud, A. (2015). Removal of Lead ions from Industrial Wastewater: A Review of Removal Methods. *International Journal of Epidemiologic Research, 2*(2), 105-109.

Mondal, M. (2009). Removal of Pb (II) ions from Aqueous Solution using Activated Tea Waste: Adsorption on a Fixed-Bed Column. *Journal of Environmental Manegement, 90*(11), 3266-3271.

National Environmental Standard and Regulations Enforcement Agency. (2009). *National Environmental Regulations.* Abuja: The Federal Government Printer.

Nwabanne, J., Okoye, A., & Lebele-Alawa, B. T. (2011). Packed Bed Column Studies for the Removal of Lead (II) using Oil Palm Empty Fruit Bunch. *European Journal of Scientific Research, 63*(2), 296-305.

Uzoije, A., & Uche, C. (2016). Studying and Modeling Dynamic Adsorption of Lead (II) ion onto Fixed Bed Column of Activated Carbon of Plantain Peels and Bamboo. *Science Journal of Environmental Engineering Research.*

Copyright © 2019 – 2021 JNET-RSU, All right reserved

Table 3: Parameters of Bohart Adams model under column adsorption process

Co (mg/l)	Qw (ml/min)	Z (cm)	MA (g)	KBA (l/min.mg)	No (mg/l)	R^2
10	5	5	168.5	0.00033	116.642	0.9141
50	5	5	167.9	0.00006	482.640	0.8701
100	5	5	168.2	0.00002	836.811	0.8315
1.426	5	5	169.0	0.00154	22.853	0.9601
1.426	7	5	168.4	0.00182	25.328	0.9798
1.426	10	5	168.0	0.00168	33.556	0.9724
1.426	5	3	101.8	0.00190	23.614	0.9438
1.426	5	5	168.6	0.00189	18.070	0.9890
1.426	5	7	227.2	0.00141	18.6701	0.9760

Table 4: Parameters of Yoon and Nelson model under column adsorption process

Co (mg/l)	Qw (ml/min)	Z (cm)	MA (g)	KYN (min^{-1})	τ(min)	R^2
10	5	5	168.5	0.00571	201.32	0.9619
50	5	5	167.9	0.00690	98.17	0.9521
100	5	5	168.2	0.01001	-0.49	0.9525
1.426	5	5	169.0	0.00371	263.78	0.9661
1.426	7	5	168.4	0.00470	184.21	0.9952
1.426	10	5	168.0	0.00501	125.18	0.9918
1.426	5	3	101.8	0.00641	88.59	0.9867
1.426	5	5	168.6	0.00510	186.02	0.9965
1.426	5	7	227.2	0.00321	325.56	0.9735

Table5: Parameters of Thomas model under column adsorption process

Co (mg/l)	Qw (ml/min)	Z (cm)	MA (g)	K_{Th} (l/mg.min)	q_{Th} (mg.ml/g.l)	R^2
10	5	5	168.5	0.00057	59.741	0.9619
50	5	5	167.9	0.00014	145.680	0.9521
100	5	5	168.2	0.00011	-1.454	0.9526
1.426	5	5	169.0	0.00260	11.160	0.9658
1.426	7	5	168.4	0.00331	10.902	0.9953
1.426	10	5	168.0	0.00351	10.583	0.9918
1.426	5	3	101.8	0.00451	6.189	0.9867
1.426	5	5	168.6	0.00372	7.936	0.9921
1.426	5	7	227.2	0.00224	10.217	0.9736

Copyright © 2019 – 2021 JNET-RSU, All right reserved

Table 6: Parameters of Clarkmodel under column adsorption process

Co (mg/l)	Qw (ml/min)	Z (cm)	MA (g)	r (min^{-1})	A	R^2
10	5	5	168.5	0.00690	7.3681	0.9521
50	5	5	167.9	0.00781	4.0597	0.9423
100	5	5	168.2	0.01062	1.7704	0.9518
1.426	5	5	169.0	0.00452	5.9390	0.9654
1.426	7	5	168.4	0.00560	5.1542	0.9931
1.426	10	5	168.0	0.00581	3.8183	0.9901
1.426	5	3	101.8	0.00720	3.5282	0.9826
1.426	5	5	168.6	0.00601	5.7001	0.9961
1.426	5	7	227.2	0.00402	6.4661	0.9746

Copyright © 2019 – 2021 JNET-RSU, All right reserved